Sensors and Actuators A 259 (2017) 137–143

Contents lists available at ScienceDirect

Sensors and Actuators A: Physical

journal homepage: www.elsevier.com/locate/sna

Measurement of average particle size in metal powders by microwave cavity perturbation in the magnetic field

N. Clark [a,*], N. Jones [b], A. Porch [a]

[a] Centre for High Frequency Engineering, Cardiff University, Cardiff, CF24 3AA, United Kingdom
[b] Renishaw Plc, New Mills, Wotton-under-Edge, Gloucestershire, GL12 8JR, United Kingdom

ARTICLE INFO

Article history:
Received 29 November 2016
Accepted 31 March 2017
Available online 1 April 2017

Keywords:
Microwave
Cavity perturbation
Metal powder
Eddy current
Magnetic
Permeability

ABSTRACT

The magnetic absorption of metallic powders, particularly at microwave frequencies, is of great theoretical and practical interest and has been the subject of previous research examining the dependence of absorption on the ratio of the particle skin depth to radius. Here, the validity of the theoretical approach concerning the peak in the absorption spectrum is verified using a 3D simulation of a hexagonal, close-packed particle matrix. Clear experimental data is given for the real and imaginary parts of the magnetic permeability of metal alloy powders (Ti6Al4V), of varying size, obtained by using the cavity perturbation technique across three separate frequencies in the GHz range. The results are shown to be congruent with existing theory. Further verification of the absorption peak is given by the testing of the powder at lowered conductivity by elevating the temperature. The results demonstrate the applicability of the relatively simple microwave cavity perturbation approach to the determination of the average particle size in a metal powder when compared with other, more complex and time-consuming methods.

1. Introduction

Since the first demonstration of sintering a metal powder body by microwave radiation [1], efforts to understand the energy absorption of conducting metal powders has been ongoing. Whilst the simple need to generate heat has been the primary concern when approaching this subject, there is much value in considering other measurement applications. For instance, from accurate knowledge of the absorption behavior of an unknown metal powder, the approximate mean particle size can be determined, or particle sizes between batches of powder can be compared.

The theoretical basis for electromagnetic absorption in conducting metal powders is well established. A variety of studies have taken a first principles approach to the absorption of an individual particle within both electric and magnetic fields [2–4]. It is accepted that, for any practical size of particles which are considered to be metallic on the basis of a high value of electrical conductivity, magnetic absorption via eddy current loss is much greater than loss in an equivalent electric field and this has been demonstrated experimentally [5,6].

Typically, studies are interested in energy absorption for the application of heating a powder. With this in mind, previous works have been undertaken to experimentally verify the absorption in metallic powders by applying high power microwave radiation and measuring the powder temperature. This has been done relatively successfully by measuring the temperature gradients and maximum temperature achieved [7]. The peak absorption rates, as predicted at specific particle sizes by theory, have also been observed experimentally [8,9]. However, using the temperature as a measure of the absolute absorption has many difficulties. Firstly, the precise power delivered to the sample must be calculated and this may not be trivial due to the complex loading and changing condition of the applicator caused by the heated powder. Also, accurate determination of other powder characteristics will likely be difficult. For instance, the powder thermal conductivity and dissipation rates can be massively affected by the ambient conditions, such as initial temperature and airflow, and other powder characteristics such as packing density, sample size and chemical composition.

Microwave cavity perturbation provides a convenient and potentially easy method of determining the absolute absorption of a powder and, using cavity modes which isolate the electric and magnetic fields at the sample insertion point, magnetic and electric absorption can be measured separately [10–13]. High Q cavities and modern network analyzers ensure that measurement

* Corresponding author.
E-mail address: clarkns@cardiff.ac.uk (N. Clark).

http://dx.doi.org/10.1016/j.sna.2017.03.037

error is extremely small and modern simulation tools have allowed for accurate correction of errors caused by sample holes and coupling structures [14]. Also, sample preparation is minimal and the technique is flexible to allow measurement at significantly elevated temperature. Another advantage is the use of multiple modes to provide simultaneous measurements at different frequencies [15]. This gives a range of microwave skin depths, which is crucial to determining the mean particle size from magnetic absorption (i.e. due to eddy currents) in metallic particles.

Determination of the particle size distribution for a powdered material is currently a relatively expensive or inconvenient process. In an industrial setting, a survey using scanning electron microscopy (SEM) is usually prohibitively expensive. Laser diffraction is the standard measurement used but this usually requires that the powder is well-dispersed in liquid, a process which in metals is prone to error due to its high density. Furthermore, these systems require significant ongoing maintenance and replenishment of consumables which makes them unattractive for many applications. Conversely, microwave cavity perturbation could provide a convenient method which relies on a simple metal structure for the cavity, and solid-state electronics to interrogate it. Information regarding the average particle size of a metallic powder can then be obtained non-destructively. The information it provides, although not a detailed particle size distribution (PSD), can be useful, for instance, in determining the evolution of powder properties over time.

2. Background

2.1. Theory

The complex magnetic dipole moment for an individual spherical particle is derived as [2]

$$m = 2\pi a^3 H_0 \left(\frac{(\mu+2)\left(1 - ka\cot(ka) - \mu(ka)^2\right)}{(\mu-1)\left(1 - ka\cot(ka) - \mu(ka)^2\right)} \right) \tag{1}$$

where a is the particle radius, H_0 is the applied magnetic field strength, ε is the internal sphere permittivity, μ is the internal sphere permeability and the wavenumber $k = \frac{\omega\sqrt{\varepsilon\mu}}{c}$. Electrical conductivity σ is introduced by making ε complex, i.e. by considering $\varepsilon = \varepsilon_1 - j\sigma/\omega\varepsilon_0$, where the imaginary part dominates the real part ε_1 for materials considered to be weakly conducting, and certainly so for materials considered to be metallic.

This leads to simplified expressions for the power absorbed per unit volume and the real part of the relative permeability for a non-magnetic conducting powder as

$$\langle P_M \rangle = \frac{3}{4}\omega\mu_0 H_0^2 \mathrm{Im}\left(1 + \frac{3\cot(ka)}{ka} - \frac{3}{(ka)^2}\right) \tag{2}$$

$$\mu_1 = 1 - \frac{1}{2}\mathrm{Re}\left(1 + \frac{3\cot(ka)}{ka} - \frac{3}{(ka)^2}\right) \tag{3}$$

Considering the large skin depth limit, $a/\delta \ll 1$ we see that for small particles

$$\lim_{\frac{a}{\delta}\to 0} \langle P_M \rangle = \frac{1}{20}\omega^2\mu_0^2 a^2 \sigma H_0^2 \propto \omega^2 a^2 \sigma \tag{4}$$

Conversely, in the small skin depth limit, we see that for large particles

$$\lim_{\frac{a}{\delta}\to \infty} \langle P_M \rangle = \frac{9}{4a}\sqrt{\frac{\omega\mu_0^2}{2\sigma}} H_0^2 \propto \frac{1}{a}\sqrt{\frac{\omega}{\sigma}} \tag{5}$$

As can be seen, for fixed value of frequency, the absorption in large particles is inversely proportional to the particle radius and proportional to the square of the radius for small particles. This reveals an absorption peak which is found when the radius is 2.4 times as large as the skin depth.

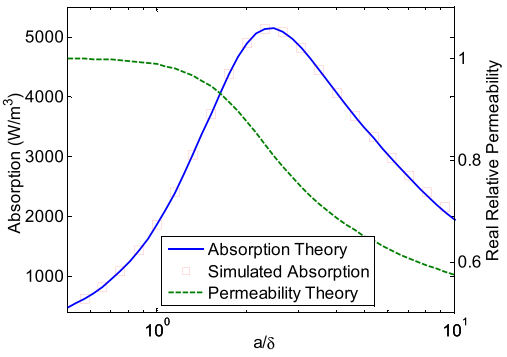

Fig. 1. Comparison of simulation and theory of the absorption and permeability of a single spherical particle. Theory curves are given by Eqs. (2) and (3).

The above results are for isolated spheres, so a key assumption is that the particles are arranged suitably sparsely such that local magnetic field corrections caused by particle-particle interactions can be ignored. However, meeting this criterion in reality is difficult due to the nature of the powder itself. Attempts to suspend the powder in some type of setting liquid are unlikely to be successful due to the high density of the individual metal particles, thus leading to particle settling. The relevance of the equations is therefore in question but this can be answered, to some extent, with simplified simulations.

2.2. Simulation

Simulations were undertaken using COMSOL Multiphysics at 2.45 GHz using a quasi-static approximation. A uniform magnetic field of amplitude 1 A/m was applied in a region of space with boundaries kept suitably far away from the particles such that the magnetic field at the boundary is unaffected by local field corrections owing to the particles. This condition mirrors the assumption made when applying first order perturbation theory. The simulations are not intended to completely characterize the absorption for multi-particle systems but simply give an indication of their behavior. In order to characterize the absorption empirically, many different packing schemes would need to be considered as well as various field orientations. In the first instance and for this case, a simple hexagonal close packed (HCP) system was used as it gives a relative packing density close to what was measured during experimentation (~0.6). The particle radius is fixed at 20 μm and the electrical size is changed by adjusting its conductivity – thus changing the ratio of skin depth to particle radius. Initially a single particle was simulated to verify future simulations, as shown in Fig. 1. The simulation shows very good agreement with the analytical theory, demonstrating the characteristic absorption peak when $a = 2.4\delta$. For completeness, the theoretical real permeability is shown, even though this was not calculated by simulation.

The next 3D simulation considers a hexagonally close packed matrix of 216 particles (i.e. a $6 \times 6 \times 6$ array). The generated particle agglomeration can be seen in Fig. 2. Note the axis directions, which are referred to later. The HCP planes are stacked in the z direction.

Four distinct conditions are considered: the field applied in either x or z direction and with the particles either touching or with a 0.1 μm gap separating all particles. The z direction indicates field application perpendicular to the 6 HCP planes. Fig. 3 shows the result of these simulations with the touching a separated cases showing distinct results. With small inter-particle separation, the measured absorption closely resembles the profile predicted by the

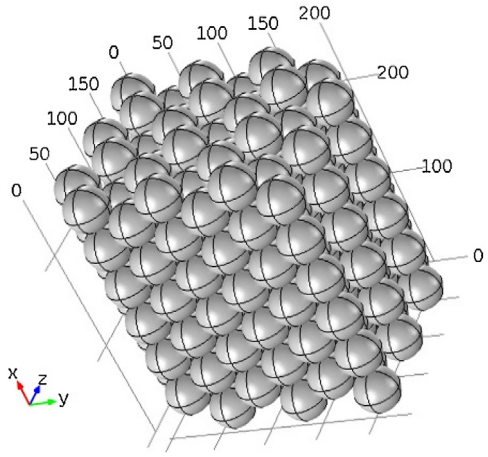

Fig. 2. HCP particles generated for COMSOL simulation.

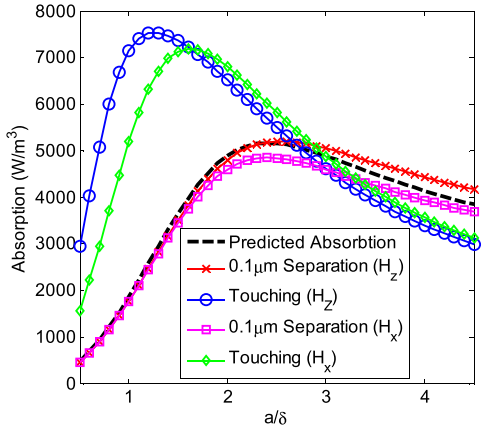

Fig. 3. Simulation of magnetic absorption per unit volume based on a 216 particle HCP array.

earlier theory. This is enabled by total magnetic field penetration in the space between particles.

Fig. 4 shows the magnetic field distribution on the cross section drawn through the middle of the particles in both the separated and touching cases. The radius is 6 times the skin depth and the magnetic field is applied in the z direction, i.e. perpendicular to the plane of the image. As previously mentioned, the separated case allows total field penetration. However, with no separation, electrical contacts between particles enable macro currents to flow in the

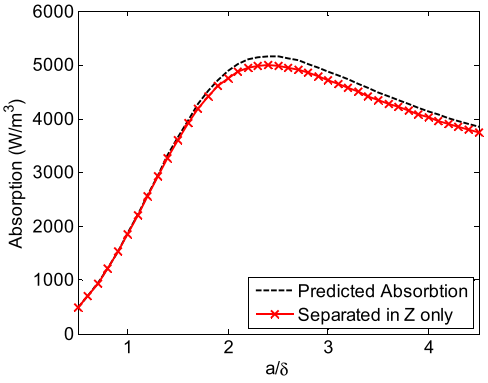

Fig. 5. Simulated magnetic absorptions based on the 216 particle HCP array. Stacked layers have been separated.

agglomeration. These currents screen the inner particles and cause a different absorption characteristic. This can be interpreted as the small particles combining to effectively increase the particle size. The peak absorption per unit volume is consequently increased, due to the voids becoming effectively trapped by the contacting particles.

It is important to note that these currents flow in a perpendicular direction to the applied magnetic field. Therefore, only contacts made in the direction perpendicular to the applied field contribute to the overall screening affect. This can be demonstrated by considering the same 216 particle matrix with the field applied in the x direction but with the HCP planes slightly separated, thus eliminating any electrical contacts in the z direction. Fig. 5 shows the absorption characteristic which closely matches the theoretical prediction. Since the compressive weight of the powder will cause electrical contacts to form above and below the particles, as long as the magnetic field is applied along the same direction as gravity, these contacts will be relatively inconsequential.

A further interesting effect is also observed when considering small particle agglomerations. A touching $3 \times 3 \times 3$ HCP was constructed and simulated with field applied in the z direction. Fig. 6 shows the results and, in contrast to the larger case, the per unit volume absorption still exhibits a peak in a similar location but the absorption is significantly increased in magnitude.

To conclude the initial simulation study, it is hypothesized that, as long as electrical contact is not made between particles, a relatively large group of closely packed particles will share the absorption behavior of a single particle up to (and close to) the absorption peak. The isolation between particle contacts in the plane perpendicular to the magnetic field can be provided by the

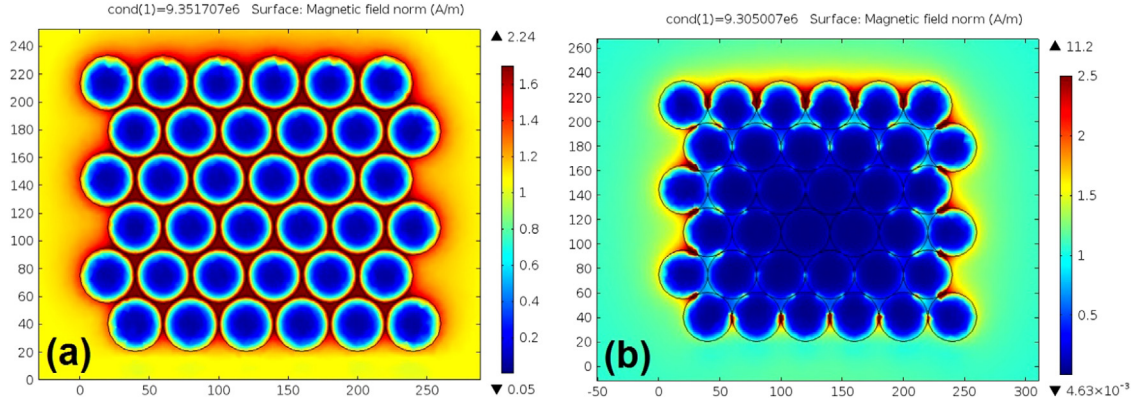

Fig. 4. Simulated magnetic field strength cross-section, taken in the xy plane through the third particle layer. (a) Separated HCP particle matrix. (b) Touching HCP particle matrix.

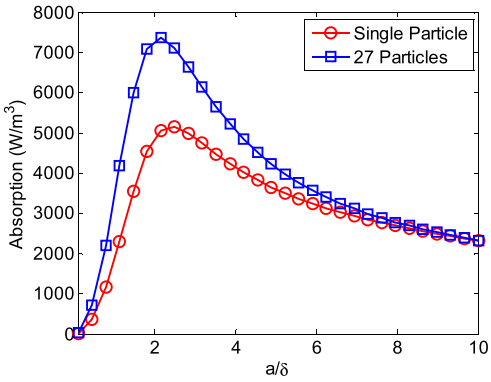

Fig. 6. Comparison of single particle absorption and simulated magnetic absorption based on a 3 × 3 × 3 HCP particle matrix.

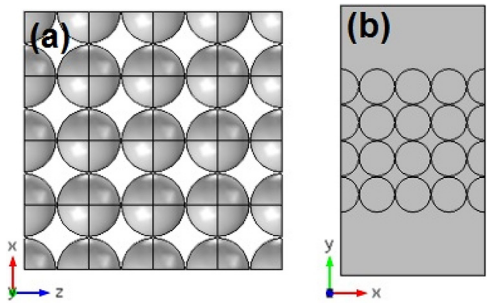

Fig. 7. Cubic close pack 3D simulation model with periodic boundaries across x and z showing the maximum 4 layers.

native oxide layer that will be present on the surfaces of the most commonly used metals. It is not expected that this oxide layer itself will contribute significantly to the magnetic absorption, as reported previously [16].

Similarly to previous studies [3,17], an effort was made to simulate an infinitely large configuration by utilizing the simple symmetry of a cubic close packed system and a periodic boundary condition (density = 0.52). Fig. 7 shows the 3D model created for simulation where the excitation ports are placed at the y limits and a periodic condition applied at the x and z limits. As defined by the periodic boundary conditions, the simulation is continuous across the x and z boundaries. In the y direction, the simulation is finite. Simulations of up to 4 layers in this direction are considered, where the number of layers is denoted by N. The boundaries at y are places sufficiently far away such that they do not influence local field distortions caused by the particles. Adjusting the distance between the particles and simulation boundary did not significantly affect simulation results.

The absorption is shown in Fig. 8, presented as the average absorption in the center 9 × N particles. It can be seen that, while the curves retain the approximate characteristic shape of absorption, significant reduction of loss is observed as the particles increase in size. This result is similar to the previously cited studies. Whilst a slight decrease in absorption can be seen for 1 layer, subsequent simulations show very similar results, thus adding confidence that the result is scalable to larger geometries.

3. Experimental setup

The cavity used was cylindrical in design with an internal radius 4.75 cm and height 4 cm, machined from aluminium. A hole is placed on its axis, with suitable RF chokes at either end, to act as a mode trap for degenerate TM modes (explicitly TM_{111}, TM_{112} and TM_{122} in this case). Furthermore, as previously described, by

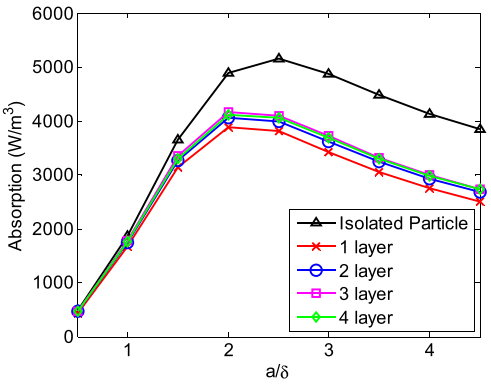

Fig. 8. Simulated absorption for multi-layer cubic close pack configuration with periodic boundary condition.

Table 1
Cavity modes utilized for measurement (Q_0 is the quality factor of the empty cavity).

Mode	Frequency (GHz)	Q_0	G_{nmp}
TE_{011}	5.36	20,062	0.284
TE_{012}	8.39	17,917	0.490
TE_{022}	10.2	26,711	0.128

exploiting different resonant modes, a sparse frequency spectrum can be obtained. As well as changing the absolute absorption for particular particle sizes, this shifts the absorption peak due to the changing skin depth. Table 1 shows the different modes utilized and their measured resonator parameters (the mode scaling constants *G* are defined below).

Cavity coupling was achieved using two near-identical, co-axial loops fed through the flat, top cavity surface. Resonator Q and resonant frequency were obtained, simultaneously, from all the modes, from measurements of the voltage transmission coefficient S_{21} in the frequency domain using an Agilent PNA-L (N5232A) utilizing a circle and linear fit strategies, as detailed elsewhere [18]. This method, using a very small span of points around the center frequency, was found to be more robust compared to a simple Lorentzian fit of the magnitude data. This is especially true for the higher order modes where distortion of the resonances due to cross-coupling becomes significant.

The per unit volume magnetic power absorption (in W/m^3) is given as

$$\langle P_M \rangle = \frac{\omega}{2}\mu_2\mu_0 H_0^2.\beta \tag{4}$$

where β is the relative density of the powder sample. The imaginary part of permeability can be obtained through standard perturbation as [14]

$$\mu_2 \approx \left(\frac{1}{Q_0} - \frac{1}{Q_S}\right)\frac{V_C}{V_S}G_{nmp} \tag{5}$$

where Q_0 is the initial resonator quality factor, Q_s is that with the sample, V_C is the cavity volume, V_S is the sample volume and G_{nmp} is a mode dependent scaling constant. The G values can be determined experimentally or via simulation, as demonstrated by Cuenca et al. using a COMSOL simulation [19].

The real permeability was also measured using the frequency shift of the resonant cavity [14].

$$\mu_1 \approx \left(\frac{f_0 - f_s}{f_0}\right)\frac{V_C}{V_S}G_{nmp} + 1 \tag{6}$$

The samples selected for testing were made from gas atomized Ti6Al4V powder obtained from the manufacturer LPW Technology Ltd. Ti6Al4V is a common Titanium alloy frequently used in aerospace and medical applications due to its high strength and

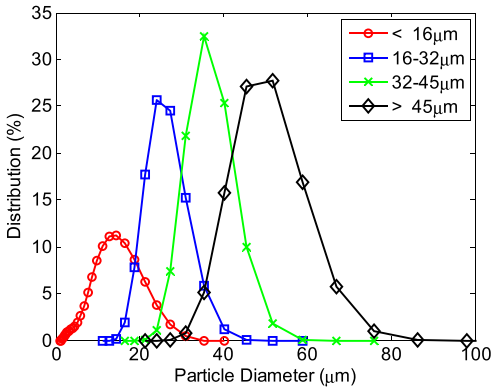

Fig. 9. Particle size distribution of fractioned Ti6Al4V powder.

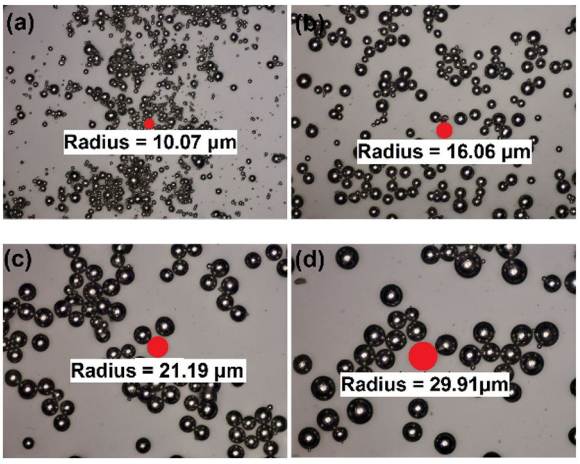

Fig. 10. Optical microscope images of fractioned Ti6Al4V powder. (a) <16 μm. (b) 16–32 μm. (c) 32–45 μm. (d) >45 μm.

biocompatibility [20]. Chemically, it is composed of 6% Aluminium, 4% Vanadium and 90% Titanium.

As Ti6Al4V is not usually used for its conductive properties, there is uncertainty regarding its conductivity. However, the bulk conductivity is assumed to be approximately 6×10^5 S/m [21]. The standard powder is described by the manufacturer to have particles with diameters in the range 16–45 μm and was progressively sieved into 4 separate powder fractions. The resultant particle size distributions (PSD), obtained from a Malvern Mastersizer 3000, can be seen in Fig. 9.

The three larger fractions appear approximately symmetrical, however, the smallest is broader. This similarity is also shown in the physical look and feel of the powders. The three larger fractions appear identical: light grey in colour and smoothly flowing. However, the smaller fraction is slightly darker and tends to form powder clumps. Imaging the separate fractions with optical microscopy utilizing focus stacking illustrates the cause of this difference. Fig. 10 shows the four particle fractions at ×20 magnification. In each case, the radius of a single highlighted particle has been measured to illustrate the relative size of the particles in each fraction. Firstly, the images reveal the powder particles are highly spherical, adding confidence that the previous analysis will be valid. Secondly, whilst small satellite particles are visible in all fractions, the smallest fraction shows a large concentration of these small sub-micron size particles. In this fraction, each larger particle is surrounded by many very small particles which appear to then cause clumps of small particles to form.

Samples were prepared by placing them into fused quartz tubing (obtained from CM Scientific Ltd, UK) with 1 mm ID and 1.2 mm OD. Subsequently they were vibrated for 10 s on a basic vibration platform at 100 Hz. The sample was not seen, visually, to compact any further for longer vibration durations. This ensured the removal of any air pockets and, as a result, resulted in uniform density. For a tall sample, significant granular convection is not expected but the vibration time is kept intentionally minimal to avoid any potential error. The samples were weighed, accurate to ±0.001 g, and the relative density calculated given the bulk density of Ti6Al4V of 4.43 g cm^{-3} [22]. Details of the 4 samples can be seen in Table 2.

Furthermore, in order to provide further verification, measurements were taken with varying metal conductivity by elevating the temperature. The sample and cavity were placed entirely in an oven (Memmert UF30Plus) and the temperature risen slowly to 150 °C and back to room temperature over 5 h ensuring uniform heating in the sample and cavity. The changes in cavity Q were accounted for by performing the experiment initially without a sample and using this as a baseline measurement. The temperature was measured using a PT-100 RTD platinum resistance thermometer, in contact with the metal cavity surface.

Table 2
Fractioned Ti6Al4V powder characteristics.

Fraction	Average Particle Diameter (μm)	Effective Density
<16 μm	13.2	0.54
16–32 μm	25.8	0.58
32–45 μm	36.1	0.58
>45 μm	47.9	0.60

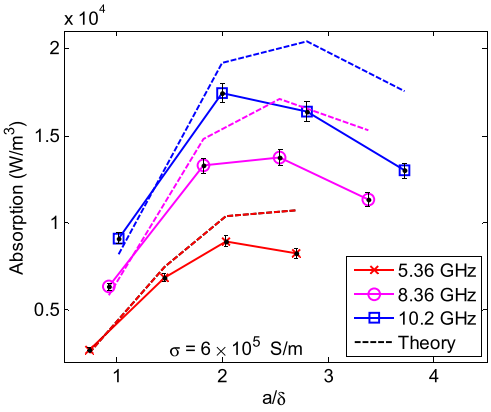

Fig. 11. Measured magnetic absorption of Ti6Al4V fractioned powder samples using cavity perturbation.

4. Experimental results

The absorption results can be seen in Fig. 11. A set of predicted values were obtained by performing a weighted sum of the absorption given by Eq. (2) over the entire PSD. The particle size for each fraction is taken as the average particle size within the distribution. The model appears to accurately predict the absorption profile of the powder. The absorption peak is observed and is seen to be at a fixed skin depth ratio.

Data for the real relative permeability, plotted alongside a set of theoretical curves given by Eq. (3), are shown in Fig. 12.

The errors plotted are the combination of the random errors encountered in Q and frequency measurement and other systematic errors. The vast majority of the error is caused from a conservative uncertainty in the mode scaling factor G (~2%) and the measurement error in sample volume used to calculate the powder density.

Fig. 13 below considers the absorption characteristic of particles at some initial conductivity and then at a second, somewhat

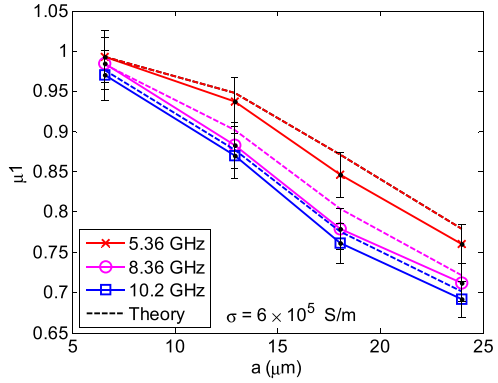

Fig. 12. Measured real permeability of Ti6Al4V fractioned powder samples using cavity perturbation.

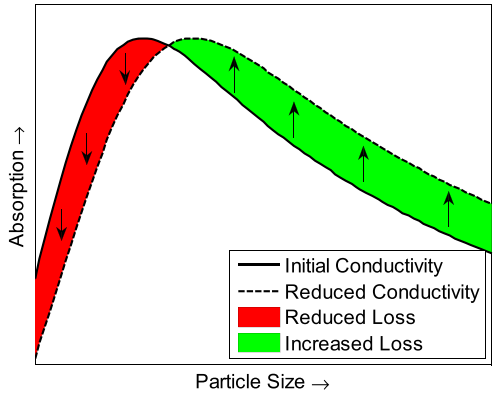

Fig. 13. Changing theoretical magnetic absorption characteristic of metallic powder if conductivity is reduced by heating.

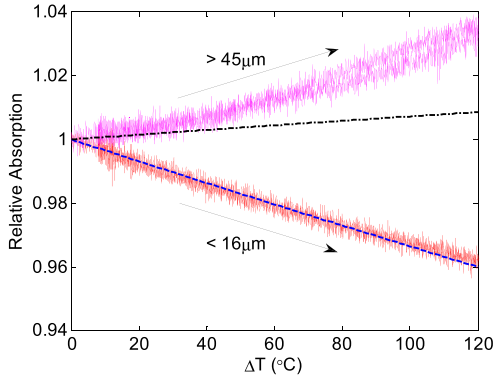

Fig. 14. Evolution of magnetic absorption with changing temperature, measured using the cavity's TE_{011} mode at 5.35 GHz within an oven.

smaller, conductivity. For the illustration the effect has been exaggerated but it can be seen that if one considers specific particle sizes, the loss can either increase or decrease as the skin depth changes. For particles above a certain size, a reduction in conductivity would result in an increase in loss and, conversely, for smaller particles the reduction results in a reduction in loss.

Finally, Fig. 14 shows the changing relative absorption of the powder as it is heated and its conductivity reduced. Theoretical curves were constructed given the temperature co-efficient of conductivity for Ti6Al4V as 0.0004/°C and an initial, room temperature, conductivity of 6×10^5 S/m. As predicted by the model, with decreasing conductivity and, as a result, an increasing skin

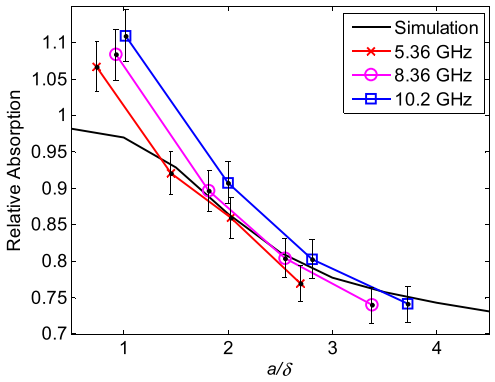

Fig. 15. Measured magnetic absorption of the Ti6Al4V fractioned powder samples given relative to the theoretical single isolated particle case. The simulation curve represents the result from the 4 layer, periodic, cubic close pack simulation.

depth, the smaller particles show reduced absorption and the larger particles increased absorption.

5. Discussion

The frequency shift and resultant real permeability shows a strong negative trend with increasing particle size. Within this range, the values appear consistent with those predicted by the presented theory.

The measured loss values also show strong correlation with the theory. Fig. 15 shows the measured relative absorption compared with the single theoretical isolated particle case. A curve is also given showing the result of the cubic close pack periodic simulation. Consistent with the simulation, the larger fractions show relatively reduced absorption with increased particle size. However, the smaller fraction, where the majority of particles are below the skin depth limit, do not follow the trend exhibiting enhanced absorption per unit volume.

This outlier can be explained by the previously mentioned differences of this powder fraction. Firstly, the particles have a tendency to cluster together. Assuming these clusters form electrically connecting networks, the result of this is an increased effective particle size without, however, a corresponding increase in weight. Therefore, the absorption per unit volume is seen to increase. This effect was demonstrated in the earlier simulation in the case of touching particles. Secondly, this fraction has a concentrated proportion of very small particles many of which are small pieces of debris formed during the gas atomization process. Particles forming this debris are less likely to be spherical in nature and therefore less likely to conform to theoretical predictions.

Comparing the two temperature dependency plots given in Fig. 14, the small particle case can be seen to closely match the predicted trend. The larger particle case, although initially following the prediction, proceeds to exhibit enhanced absorption. This is a surprising result but one that can be explained by the earlier simulation. During heating, the particles will thermally expand. Although this expansion is relatively small, not causing significant change to the electrical size, it will cause an increased density of electrical contacts. The increased density of contacts is not sufficient to cause a reduction of the absorption caused by screening but the contacts create small particle agglomerations which show increased absorption per unit volume, as demonstrated by the earlier simulation. It is expected that this behavior will be strongly dependent on the sample container geometry.

6. Conclusion

The cavity perturbation method has proven to be a convenient and insightful method for considering the magnetic absorption of a conducting metal powder. Given these results, it is conceivable to construct a cheap and simple sensor based on microwave perturbation in order to assess evolution of particle size of a powder within an industrial process or to simply assess a powder with the intention of microwave heating. Reduced absorption, compared with the single particle case, was observed in all cases for particles bigger than the skin depth. However, the absorption peak was relatively unchanged and, within the tested range, absorption was no worse than 75% of the ideal case. When heating the powder, some nonlinear behavior was observed at high temperature due to particle thermal expansion causing particle agglomeration.

Acknowledgments

NC gratefully acknowledges the funding of Renishaw and the UK Engineering and Physical Sciences Research Council (EPSRC) via its ICASE studentship programme.

References

[1] R. Roy, D. Agrawal, J. Cheng, S. Gedevanishvili, Full sintering of powdered-metal bodies in a microwave field, Nature 399 (1999) 668–670.
[2] A. Porch, D. Slocombe, P.P. Edwards, Microwave absorption in powders of small conducting particles for heating applications, Phys. Chem. Chem. Phys. 15 (2013) 2757–2763, http://dx.doi.org/10.1039/c2cp43310a.
[3] M. Ignatenko, M. Tanaka, M. Sato, Absorption of microwave energy by a spherical nonmagnetic metal particle, Jpn. J. Appl. Phys. 48 (2009) 67001, http://dx.doi.org/10.1143/jjap.48.067001.
[4] K.I. Rybakov, V.E. Semenov, S.V. Egorov, A.G. Eremeev, I.V. Plotnikov, Y.V. Bykov, Microwave heating of conductive powder materials, J. Appl. Phys. 99 (2006) 23506, http://dx.doi.org/10.1063/1.2159078.
[5] J. Cheng, R. Roy, D. Agrawal, Experimental proof of major role of magnetic field losses in microwave heating of metal and metallic composites, J. Mater. Sci. Lett. 20 (2001) 1561–1563.
[6] J. Ma, J.F. Diehl, E.J. Johnson, K.R. Martin, N.M. Miskovsky, C.T. Smith, G.J. Weisel, B.L. Weiss, D.T. Zimmerman, Systematic study of microwave absorption, heating, and microstructure evolution of porous copper powder metal compacts, J.Appl. Phys. 101 (2007) 74906, http://dx.doi.org/10.1063/1.2713087.
[7] A. Mondal, A. Shukla, A. Upadhyaya, D. Agrawal, Effect of porosity and particle size on microwave heating of copper, Sci. Sinter. 42 (2010) 169–182, http://dx.doi.org/10.2298/SOS1002169M.
[8] K. Kashimura, N. Hasegawa, S. Suzuki, M. Hayashi, T. Mitani, N. Shinohara, K. Nagata, Effects of relative density on microwave heating of various carbon powder compacts microwave-metallic multi-particle coupling using spatially separated magnetic fields, J. Appl. Phys. 113 (2013) 24902, http://dx.doi.org/10.1063/1.4772648.
[9] P. Mishra, a. Upadhyaya, G. Sethi, Modeling of microwave heating of particulate metals, Metall. Mater. Trans. B 37 (2006) 839–845, http://dx.doi.org/10.1007/s11663-006-0066-z.
[10] U. Raveendranath, K.T. Mathew, New cavity rerturbation technique for measuring complex permeability of ferrite materials, Microw. Opt. Technol. Lett. 18 (1998) 241–243.
[11] H. Kobayashi, S. Ogawa, Dielectric constant and conductivity measurement of powder samples by the cavity perturbation method, Jpn. J. Appl. Phys. 10 (1971) 345–350, http://dx.doi.org/10.1143/JJAP.10.345.
[12] D.T. Zimmerman, J.D. Cardellino, K.T. Cravener, K.R. Feather, N.M. Miskovsky, G.J. Weisel, Microwave absorption in percolating metal-insulator composites, Appl. Phys. Lett. 93 (2008) 214103, http://dx.doi.org/10.1063/1.3036900.
[13] M. Lin, Y. Wang, M.N. Afsar, Precision measurement of complex permittivity and permeability by microwave cavity perturbation technique, in: Joint 30th International Conference on Infrared and Millimeter Waves and 13th International Conference on Terahertz Electronics, 2005, IRMMW-THz, 2005 http://ieeexplore.ieee.org/document/1572407/.
[14] J.A. Cuenca, E. Thomas, S. Mandal, O. Williams, A. Porch, Broadband microwave measurements of nanodiamond, in: Microw. Conf. (APMC), 2014 Asia-Pacific, Sendai, Japan, 2014, pp. 441–443.
[15] J.A. Cuenca, E. Thomas, S. Mandal, O. Williams, A. Porch, Investigating the broadband microwave absorption of nanodiamond impurities, 63 (2015) 4110–4118. 10.1109/TMTT.2015.2495156.
[16] M. Ignatenko, M. Tanaka, Effective permittivity and permeability of coated metal powders at microwave frequency, Phys. B Condens. Matter. 405 (2010) 352–358, http://dx.doi.org/10.1016/j.physb.2009.08.086.
[17] T. Galek, K. Porath, E. Burkel, U. van Rienen, Extraction of effective permittivity and permeability of metallic powders in the microwave range, Model. Simul. Mater. Sci. Eng. 18 (2010) 25015, http://dx.doi.org/10.1088/0965-0393/18/2/025015.
[18] M.C. Sanchez, E. Martin, J.M. Zamarro, New vectorial automatic technique for characterisation of resonators, 136 (1989) 147–150.
[19] J.A. Cuenca, S. Klein, R. Rüger, A. Porch, Microwave complex permeability of magnetite using non-demagnetising and demagnetising cavity modes, in: 44th Eur. Microw. Conf., Rome, 2014, pp. 128–131.
[20] W.D. Callister, Materials Science and Engineering: An Introduction, 6th ed., Wiley, New York, 2003.
[21] V. Parshin, E. Serov, K. Van Klooster, R. Ravanelli, Resonator techniques for reflectivity and surface resistivity at high temperature: methodology and measurements, Int. Conf. Microw. Radar Wirel. Commun. (2010) 1–5 http://ieeexplore.ieee.org/xpls/abs_all.jsp?arnumber=5540487.
[22] Metals Handbook Volume 1, 8th ed., American Society for Metals, Novelty, Utah, 1961.

Biographies

Nicholas Clark received the B.Eng. (Hons.) degree in Computer Systems Engineering from Cardiff University, Cardiff, UK in 2013. He is currently working towards a Ph.D. at Cardiff University. He is currently concerned with the application of microwave resonant structures and his specific research interests include the characterisation and heating of metal powders and structures.

Nick Jones is a Technical Manager within Renishaw's Group Engineering Division, based at the company head office in Gloucestershire, UK. He leads a team of engineers and scientists, the Additive Manufacturing Technology and Concepts Group (AMTC), providing research and design support to the company's Additive Manufacturing Product Division in Stone, Staffordshire. He has been with the company for over twenty years, working in a number of product divisions as well as in process development and manufacturing roles. He holds B.Eng and M.Eng degrees in Mechatronic Engineering.

Adrian Porch received the M.A. degree in physics and Ph.D. degree in low-temperature physics from Cambridge University, Cambridge, U.K. He is a Professor with the School of Engineering, Cardiff University, Cardiff, U.K., and a member of the Centre for High Frequency Engineering. He has over 30 years of experience in applying microwave methods to measure and understand the fundamental properties of electronic materials. More recently, his techniques have been used to develop new types of electromagnetic sensors, with emphasis on applications across different disciplines.